Value of [^{68}Ga]Ga-NYM046 PET/CT, in Comparison with ^{18}F-FDG PET/CT, for Diagnosis of Clear Cell Renal Cell Carcinoma

Kequan Lou*[1], Jialiang Wang*[1], Huihui He[1], Yanjuan Wang[1], Yuanyuan Mi[2], Wenjin Li[3], Liping Chen[1], Yu Zhang[1], Yong Mao[3,4], Jianguo Lin[5], Haitian Fu[1,3], and Chunjing Yu[1,3]

[1]*Department of Nuclear Medicine, Affiliated Hospital of Jiangnan University, Wuxi, China;* [2]*Department of Urological Surgery, Affiliated Hospital of Jiangnan University, Wuxi, China;* [3]*Wuxi School of Medicine, Jiangnan University, Wuxi, China;* [4]*Department of Oncology, Affiliated Hospital of Jiangnan University, Wuxi, China; and* [5]*Jiangsu Key Laboratory of Molecular Nuclear Medicine, Jiangsu Institute of Nuclear Medicine, Wuxi, China*

This study aimed to investigate the diagnostic efficacy of [^{68}Ga]Ga-NYM046 PET/CT in animal models and patients with clear cell renal cell carcinoma (ccRCC) and to compare its performance with that of ^{18}F-FDG PET/CT. **Methods:** The in vivo biodistribution of [^{68}Ga]Ga-NYM046 was evaluated in mice bearing OS-RC-2 xenografts. Twelve patients with ccRCC were included in the study; all completed paired [^{68}Ga]Ga-NYM046 PET/CT and ^{18}F-FDG PET/CT. The diagnostic efficacies of these 2 PET tracers were compared. Moreover, the positive rate of carbonic anhydrase IX in the pathologic tissue sections was compared with the SUV_{max} obtained by PET/CT. **Results:** The tumor accumulation of [^{68}Ga]Ga-NYM046 at 1 h after injection in OS-RC-2 xenograft tumor models was 7.21 ± 2.39 injected dose per gram of tissue. Apart from tumors, the kidney and stomach showed high-uptake distributions. In total, 9 primary tumors, 96 involved lymph nodes, and 147 distant metastases in 12 patients were evaluated using [^{68}Ga]Ga-NYM046 and ^{18}F-FDG PET/CT. Compared with ^{18}F-FDG PET/CT, [^{68}Ga]Ga-NYM046 PET/CT detected more primary tumors (9 vs. 1), involved lymph nodes (95 vs. 92), and distant metastases (137 vs. 127). In quantitative analysis, the primary tumors' SUV_{max} (median, 13.5 vs. 2.4; $z = -2.668$, $P = 0.008$) was significantly higher in [^{68}Ga]Ga-NYM046 PET/CT. Conversely, the involved lymph nodes' SUV_{max} (median, 5.9 vs. 7.6; $z = -3.236$, $P = 0.001$) was higher in ^{18}F-FDG PET/CT. No significant differences were found for distant metastases (median SUV_{max}, 5.0 vs. 5.0; $z = -0.381$, $P = 0.703$). Higher [^{68}Ga]Ga-NYM046 uptake in primary tumors corresponded to higher expression of carbonic anhydrase IX, with an R^2 value of 0.8274. **Conclusion:** [^{68}Ga]Ga-NYM046 PET/CT offers a viable strategy for detecting primary tumors, involved lymph nodes, and distant metastases in patients with ccRCC.

Key Words: [^{68}Ga]Ga-NYM046; ^{18}F-FDG; PET/CT; carbonic anhydrase IX; clear cell renal cell carcinoma

J Nucl Med 2024; 65:1884–1890
DOI: 10.2967/jnumed.124.267527

Renal malignancies account for 2% of the annual global tumor incidence, with clear cell renal cell carcinoma (ccRCC) being predominant (*1*). The success of treating patients depends on early diagnosis and accurate staging, which are crucial in guiding personalized therapeutic management (*2*,*3*). About 20%–30% of individuals who have undergone surgery for renal cell carcinoma are at risk of metastatic relapse (*4*). Such relapses can manifest in unusual sites such as the pancreas, peritoneal cavity, and intestinal tract, which are likely to be missed by routine follow-up (*5*,*6*). ^{18}F-FDG PET/CT is a commonly used method for whole-body evaluation of tumors. Nevertheless, its performance in diagnosing primary foci of ccRCC has been disappointing, as previous metaanalyses demonstrated a sensitivity of only 62% (*7*). In addition, some studies revealed that ^{18}F-FDG PET/CT faces inherent challenges in diagnosing metastatic lesions of ccRCC because of the high physiologic background activity and inflammation, with a variable sensitivity range of 63.6%–90.0% (*8*–*10*). Consequently, these limitations underscore the need to develop alternative diagnostic strategies to improve the accuracy of tumor detection.

Carbonic anhydrase IX (CAIX) belongs to the phylogenetically well-preserved carbonic anhydrase family and is induced by hypoxia, functionally related to the acidic tumor microenvironment, involved in tumor aggressiveness (*11*,*12*). Moreover, CAIX is highly expressed in nearly all cases of ccRCC, triggered by the inactivation of von Hippel–Lindau syndrome (*13*). By contrast, CAIX expression in adult normal tissues is relatively low, except in the stomach, bile duct epithelium, and gallbladder (*14*). A CAIX-targeting mouse IgG1 monoclonal antibody (known as G250 or girentuximab) was first labeled with ^{131}I and applied as an imaging agent in patients with ccRCC (*15*). Subsequently, ^{111}In- or ^{89}Zr-girentuximab entered clinical research (*16*–*19*). However, the findings from previous studies indicated that large-molecule antibodies often exhibit limited tumor penetration and slow blood clearance. Compared with large-molecule biopharmaceuticals, small-molecule targeted drugs exhibit superior characteristics in various domains, including pharmacokinetic behavior, cost, patient adherence, and ease of drug storage and transportation (*20*).

Here, a new small-molecule compound, NYM046, targeting CAIX was introduced. It is based on acetazolamide and features a DOTA chelating structure for ^{68}Ga labeling. In this study, the diagnostic efficacy of [^{68}Ga]Ga-NYM046 in OS-RC-2 xenograft tumor models and

Received Jan. 31, 2024; revision accepted Oct. 23, 2024.
For correspondence or reprints, contact Chunjing Yu (ycjwxd1978@jiangnan.edu.cn) or Haitian Fu (phie136@sina.com).
*Contributed equally to this work.
Published online Nov. 14, 2024.

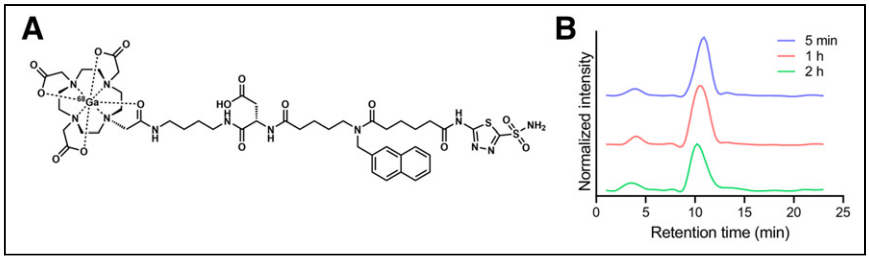

FIGURE 1. (A) Chemical structure of [^{68}Ga]Ga-NYM046. (B) Stability of [^{68}Ga]Ga-NYM046 in serum on radioactive high-performance liquid chromatography analysis.

patients with ccRCC was evaluated, and its application value was compared with that of ^{18}F-FDG PET/CT.

MATERIALS AND METHODS

Radiopharmaceutical Preparation

NYM046 was synthesized by Shanghai Bioduro Biologics Co., Ltd., by the authors' design. Radionuclide labeling was performed using the Morten M1 system (Sunmao Medical Technologies). In brief, ^{68}Ga was prepared using a ^{68}Ge/^{68}Ga generator (Eckert & Ziegler) and 0.05 M HCl (5 mL). The eluate was added to a reaction flask containing a sodium acetate buffer (0.25 M), along with 40 μg (0.036 μmol) of the precursor, NYM046 (1 mg/mL), to achieve a mixture with a pH of 4. The mixture was heated to 100°C for 10 min and purified using a C18 Sep-Pak cartridge (Waters), with 0.5 mL of 75% ethanol solution and 5 mL of normal saline as eluents. The product, [^{68}Ga]Ga-NYM046, was confirmed by radioactive high-performance liquid chromatography (Thermo Fisher Scientific, Inc.).

Small-Animal PET/CT and Blocking Study

Tumor-bearing mice were anesthetized by administration of 1.5%–2% isoflurane through an air current set at 0.5 L/min and then were intravenously injected with [^{68}Ga]Ga-NYM046 (2.3 ± 0.1 MBq, 0.2 mL). Dynamic scanning using small-animal PET/CT followed (Super Nova) within 3 h. Small-animal PET/CT images were reconstructed using 3-dimensional ordered-subsets expectation maximization. Then, the major organs were manually outlined on the images as the region of interest. The percentage injected dose per gram of tissue (%ID/g) for major organs was calculated using PMOD (version 4.3; PMOD Technologies). For blocking experiments, tumor-bearing mice were administered unlabeled NYM046 (400 μg, 0.2 mL) intravenously, followed 1 h later by an intravenous injection of [^{68}Ga]Ga-NYM046 (2.1 ± 0.1 MBq, 0.2 mL), with scanning performed at 1 h after injection. Animal experiments were performed in compliance with the guidelines established by the ethical committee of Jiangnan University.

Patient Inclusion Criteria

This study was a prospective, single-center trial to evaluate the diagnostic performance of [^{68}Ga]Ga-NYM046 PET/CT in patients with primary or metastatic ccRCC. Twelve patients were ultimately enrolled, all of whom had undergone surgery or puncture biopsy of renal lesions with a confirmed diagnosis of ccRCC (Supplemental Fig. 1; supplemental materials are available at http://jnm.snmjournals.org). The study was authorized by the Ethics Committee of the Jiangnan University affiliated hospital (LS2020003). All patients provided written informed consent to participate in the study. The study was registered at ClinicalTrials.gov (NCT05638256).

PET/CT in Patients

Each patient underwent paired [^{68}Ga]Ga-NYM046 and ^{18}F-FDG imaging using a PET/CT scanner (Siemens Biography 64 TruePoint). The interval between the 2 scans was less than 3 d. Scans were taken from the head to the upper femur and divided into separate head and body portions. The mean dose of [^{68}Ga]Ga-NYM046 was 129 MBq (range, 98–174 MBq) for each patient, whereas the dose of ^{18}F-FDG was based on the patient's weight (5.55 MBq/kg).

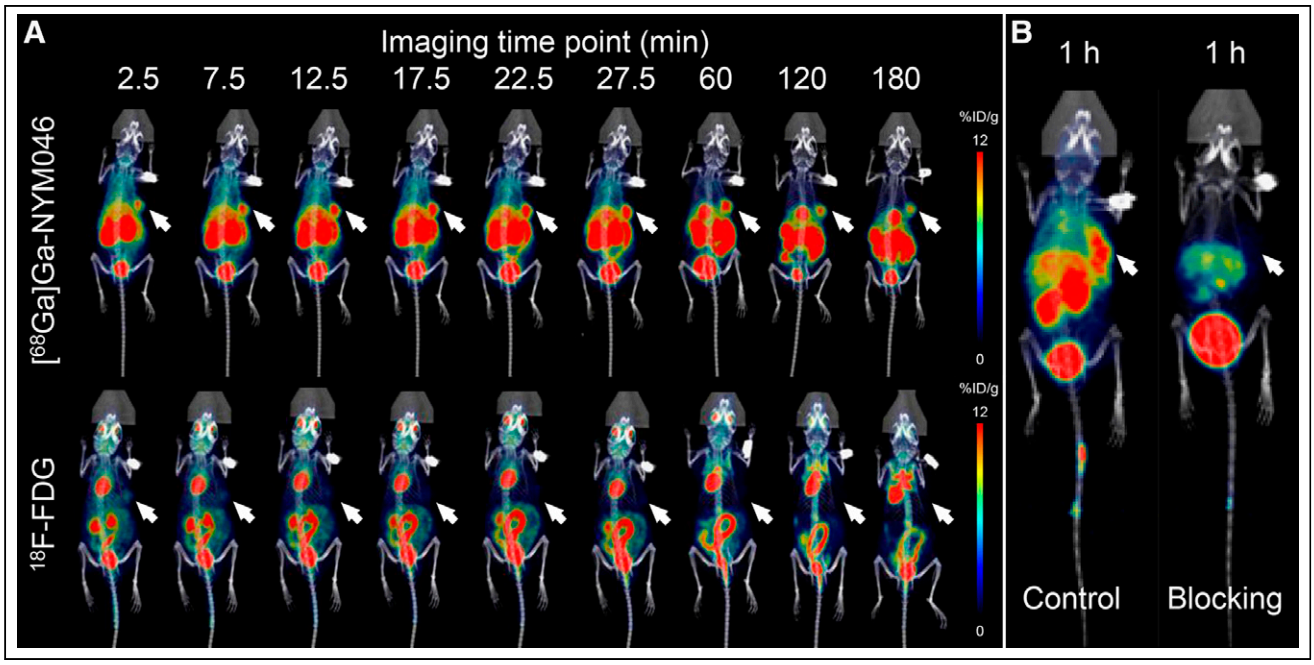

FIGURE 2. (A) In vivo biodistribution imaging of [^{68}Ga]Ga-NYM046 and ^{18}F-FDG in OS-RC-2 xenograft tumor models. (B) Representative PET/CT images of OS-RC-2 xenograft tumor models with or without unlabeled NYM046 blocking.

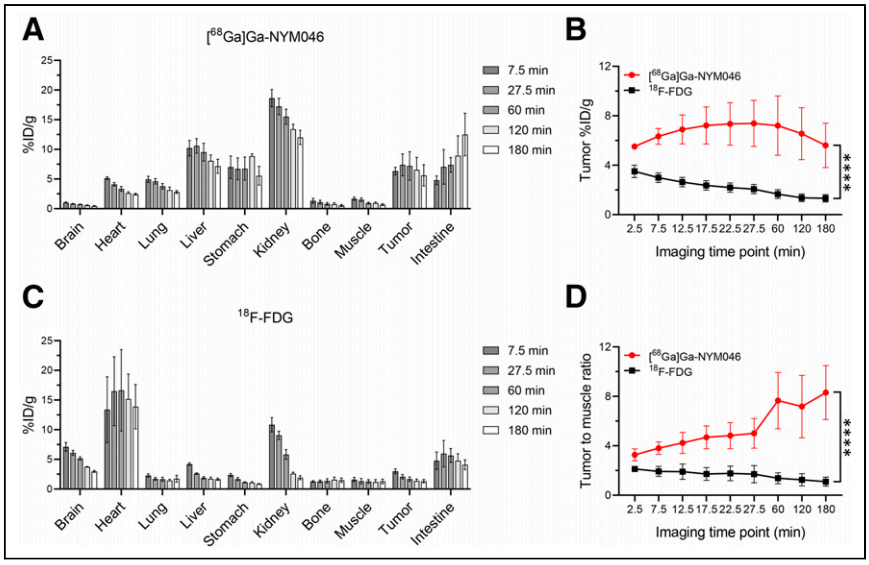

FIGURE 3. (A and C) Radioactivity biodistribution of [^{68}Ga]Ga-NYM046 (A) and ^{18}F-FDG (C) in various organs in OS-RC-2 tumor model at different time points after injection. (B and D) Quantitative curves of tumor uptake (B) and contrast (D) with background tissues (tumor-to-muscle contrast). ****$P < 0.0001$.

PET/CT Image Analysis

[^{68}Ga]Ga-NYM046 and ^{18}F-FDG PET/CT images were viewed independently by 2 qualified nuclear medicine physicians. Any lesion with higher radioactivity uptake than in the surrounding normal tissue was considered positive (except for physiologic uptake). The short diameters of involved lymph nodes and the long diameters of other measurable lesions were measured according to the RECIST 1.1 standard. SUV_{max} was obtained by outlining the region of interest.

Statistical Analysis

All statistical analyses were accomplished using SPSS 25.0 (IBM). SUV_{max} data were expressed as median, first quartile, and third quartile and were compared using the nonparametric Wilcoxon signed-rank test. Lesion numbers were assessed using the McNemar test. Statistical differences were considered significant if the P value was less than 0.05.

RESULTS

Chemistry and Radiolabeling

The chemical structure and characterization of NYM046 are shown in Supplemental Fig. 2. NYM046 exhibited a molecular mass of 1,118.45 g/mol and a purity of 95.74% (Supplemental Fig. 2). The chemical structure of [^{68}Ga]Ga-NYM046 is shown in Figure 1A, and its molar activity was 3.68 ± 0.83 GBq/μmol. The radiochemical purity of [^{68}Ga]Ga-NYM046 was more than 95% (Supplemental Fig. 3). Additionally, [^{68}Ga]Ga-NYM046 remained stable for more than 2 h in human serum (Fig. 1B). The binding affinity of [^{68}Ga]Ga-NYM046 to CAIX was 4.98 ± 0.50 nM

TABLE 1
Characteristics of Included Clinical Cases

Patient no.	Sex	Age (y)	Condition	Tumor location	Lesions*	SUV_{max} [^{68}Ga]Ga-NYM046	SUV_{max} ^{18}F-FDG
1	F	56	Preop	Primary tumor	1/0	8.2	1.9
2	F	46	Preop	Primary tumor	1/0	6.2	2.5
3	F	54	Postop	Pleura, pancreas mets	7/0	4.3 (2.6, 8.9)	2.0 (1.5, 2.4)
4	M	67	Preop	Primary tumor	1/0	3.7	2.3
5	M	63	Preop	Primary tumor	1/0	13.5	2.9
6	M	38	Preop	Primary tumor	1/0	11.5	2.6
7	M	59	Preop	Primary tumor	1/0	13.9	2.2
				Lymph node met	0/1	5.0	1.6
				Lung and bone mets	3/1	6.5 (4.1, 13.8)	2.4 (1.4, 3.0)
8	M	46	Preop	Primary tumor	1/0	13.9	2.2
9	M	72	Preop	Primary tumor	1/0	18.5	2.6
10	M	59	Postop	Lymph node mets	19/72	5.8 (4.7, 7.5)	7.8 (5.6, 9.4)
				Brain, lung, liver, bone and subcutaneous mets	55/68	4.9 (3.7, 6.5)	5.5 (4.2, 6.9)
11	M	81	Preop	Primary tumor	1/0	43.7	2.4
				Lung, adrenal gland and bone mets	5/4	11.2 (5.3, 15.3)	2.8 (1.8, 4.0)
12	M	73	Postop	Lymph node mets	3/1	21.4 (9.6, 24.9)	3.6 (2.5, 4.0)
				Lung and bone mets	2/2	13.1 (7.9, 16.9)	2.0 (1.0, 9.0)

*Measurable/nonmeasurable lesions on CT according to RESIST 1.1 standard.
Preop = before operation; postop = after operation; met = metastasis.
SUV_{max} is expressed as specific numeric value or as median followed by first and third quartiles in parentheses.

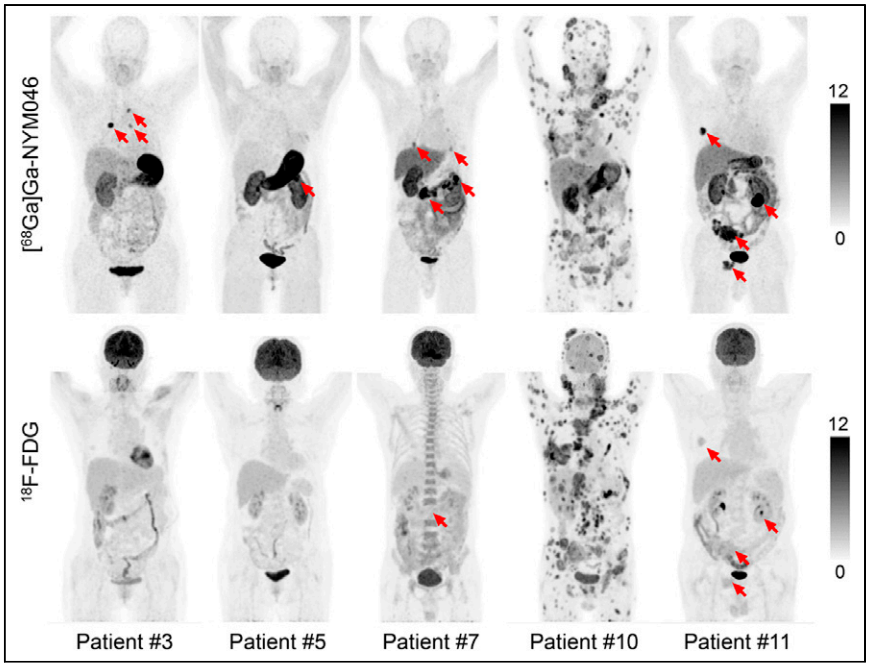

FIGURE 4. Representative maximum-intensity projections of 5 patients (patients 3, 5, 7, 10, and 11) comparing [^{68}Ga]Ga-NYM046 and ^{18}F-FDG. Both tracers showed specific retention in bone and lymph node metastases (patients 10 and 11). [^{68}Ga]Ga-NYM046 PET/CT outperformed ^{18}F-FDG PET/CT in detecting primary tumors, lung metastases, and pleural metastases (patients 3, 5, 7, and 11).

(Supplemental Fig. 4). During the safety assessment, 6 mice were injected with [^{68}Ga]Ga-NYM046 (7.4 MBq, 0.5 mL) via the tail vein, and no body weight loss was observed over 14 d (Supplemental Fig. 5).

PET/CT in Animals

The radioactivity uptake of [^{68}Ga]Ga-NYM046 in OS-RC-2 xenograft tumor models peaked between 27.5 and 60 min (Fig. 2A), and the tumor accumulation at 1 h after injection was 7.21 ± 2.39 %ID/g (Supplemental Table 1). The blockade study of [^{68}Ga]Ga-NYM046 showed a decrease in tumor radioactivity uptake from 8.66 ± 2.17 %ID/g to 2.46 ± 0.67 %ID/g for 1 h (Fig. 2B).

The radioactivity biodistributions of [^{68}Ga]Ga-NYM046 and ^{18}F-FDG in the OS-RC-2 xenograft tumor models was assessed (Figs. 3A and 3C). The tumor accumulation and tumor-to-muscle ratio were significantly higher for [^{68}Ga]Ga-NYM046 PET/CT than for ^{18}F-FDG PET/CT within 3 h (Figs. 3B and 3D).

Clinical PET/CT Studies in Patients with ccRCC

Patient clinical data are presented in Table 1. Twelve patients (9 male and 3 female; median age, 59 y; range, 38–81 y) who underwent paired [^{68}Ga]Ga-NYM046 and ^{18}F-FDG PET/CT were prospectively enrolled. No adverse reactions were observed in patients after [^{68}Ga]Ga-NYM046 PET/CT in a 2-wk follow-up period.

Representative PET/CT images of 5 patients at 1 h after injection of [^{68}Ga]Ga-NYM046 and ^{18}F-FDG are shown in Figure 4. The tissues with the highest SUV_{max} uptake of [^{68}Ga]Ga-NYM046 were the stomach (22.14 ± 16.40), tumor (8.60 ± 5.98), kidney (6.92 ± 2.24), and gallbladder (6.68 ± 2.04; Supplemental Table 2). The SUV_{max} of ^{18}F-FDG in tumor was 1.87 ± 0.48, which was lower than that of [^{68}Ga]Ga-NYM046 (Supplemental Table 2).

In visual analysis, the comparison revealed that [^{68}Ga]Ga-NYM046 PET/CT detected more primary tumors (9/9 vs. 1/9, $P = 0.008$) and distant metastases (137/147 vs. 127/147, $P = 0.041$). Meanwhile, these 2 scans had roughly similar efficacy in diagnosing lymph node metastases (Table 2). A typical image comparing the 2 scans is shown (Fig. 5). Additionally, 103 of 252 CT-measurable lesions were positive for [^{68}Ga]Ga-NYM046 uptake, or approximately 41%.

The uptake of [^{68}Ga]Ga-NYM046 and ^{18}F-FDG in all tumor lesions was further analyzed (Table 2). In primary tumors, the SUV_{max} for [^{68}Ga]Ga-NYM046 was significantly higher than that for ^{18}F-FDG (median, 13.5 vs. 2.4; $z = -2.668$, $P = 0.008$). However, a lower SUV_{max} was observed for [^{68}Ga]Ga-NYM046 PET/CT than for ^{18}F-FDG PET/CT for metastatic lymph nodes (median, 5.9 vs. 7.6; $z = -3.236$, $P = 0.001$). Moreover, no significant differences in SUV_{max} were found between the 2 agents for distant metastases (median, 5.0 vs. 5.0; $z = -0.381$, $P = 0.703$).

Patient 12, a 73-y-old man, had undergone a total right nephrectomy several years previously and was pathologically diagnosed with ccRCC (Fig. 6). During follow-up, lesions in the right adrenal gland, multiple pulmonary nodules, and enlarged mediastinal lymph

TABLE 2
Comparison of [^{68}Ga]Ga-NYM046 and ^{18}F-FDG PET/CT in Patients at 1 Hour After Injection

	SUV_{max}				Lesions (*n*)			
Parameter	[^{68}Ga]Ga-NYM046	^{18}F-FDG	*z*	*P*	[^{68}Ga]Ga-NYM046	^{18}F-FDG	χ^2	*P*
Primary tumor (*n* = 9)	13.5 (7.2, 16.2)	2.4 (2.2, 2.6)	−2.668	0.008	9	1	6.125	0.008
Lymph node metastases (*n* = 96)	5.9 (4.8, 7.8)	7.6 (5.0, 9.4)	−3.236	0.001	95	92	0.800	0.375
Distant metastases (*n* = 147)	5.0 (3.8, 7.1)	5.0 (3.7, 6.8)	−0.381	0.703	137	127	4.050	0.041

SUV_{max} is expressed as median followed by first and third quartiles in parentheses and was assessed using nonparametric Wilcoxon signed-rank test. Lesion numbers were assessed using McNemar test.

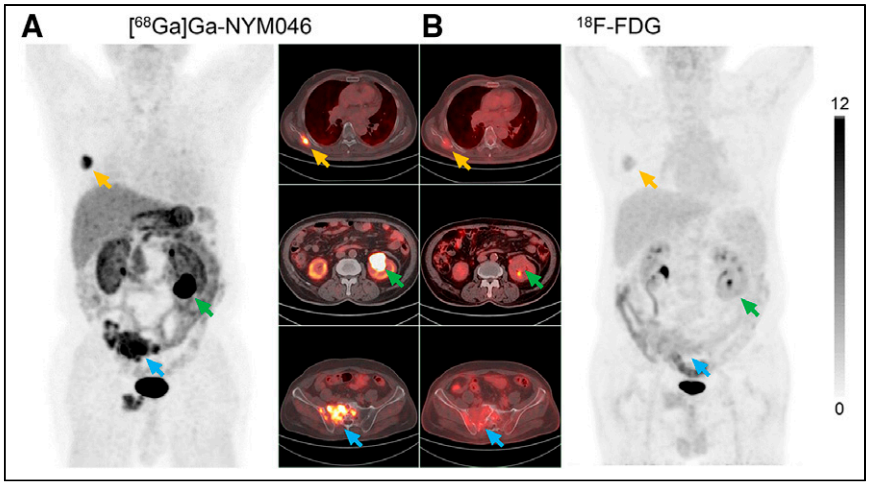

FIGURE 5. [^{68}Ga]Ga-NYM046 PET/CT (A) and ^{18}F-FDG PET/CT (B) scans of patient 11. Bone metastases (yellow and blue arrows) were diagnosed as positive findings in both scans, whereas renal primary tumor (green arrows) was diagnosed as positive finding on [^{68}Ga]Ga-NYM046 PET/CT but as false-negative finding on ^{18}F-FDG PET/CT.

nodes were identified. [^{68}Ga]Ga-NYM046 PET/CT confirmed that CAIX was highly expressed at all these sites, with an SUV_{max} of 23.9. After 2 cycles of treatment with a programmed death receptor 1 inhibitor and a protein tyrosine kinase inhibitor, posttreatment [^{68}Ga]Ga-NYM046 PET/CT showed partial shrinkage of the lesions compared with the previous CT images, as well as a significant decrease in uptake on PET.

Some patients in the study underwent nephrectomy after PET/CT, and our group obtained 6 tumor section specimens for immunohistochemical studies with the patients' informed consent. The immunohistochemical staining results revealed remarkable CAIX expression in these tumors (Supplemental Fig. 6A). Quantitative analysis showed that the higher [^{68}Ga]Ga-NYM046 uptake in primary renal tumors corresponded to higher CAIX expression, with an R^2 value of 0.8274 (Supplemental Fig. 6B).

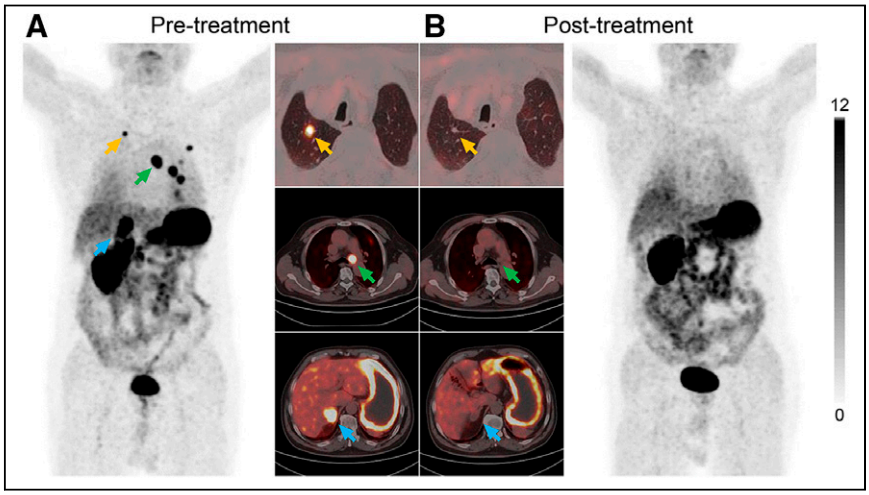

FIGURE 6. Images of patient 12 (73-y-old man), who underwent left nephrectomy with pathologically confirmed ccRCC and suspected tumor metastases on follow-up. (A) Images from pretreatment [^{68}Ga]Ga-NYM046 PET/CT demonstrate mediastinal lymph node metastases (green arrows), lung metastases (yellow arrows), and right adrenal metastases (blue arrows). (B) After 2 treatment cycles, all metastases were negative for uptake.

DISCUSSION

Renal cell carcinoma is the most common type of kidney cancer (*21*). Despite improvements in the 5-y survival rate, the prognosis for patients with advanced ccRCC remains unfavorable (*22*). Over the past 2 decades, there has been a significant evolution in the diagnosis and treatment of ccRCC, transitioning from traditional to innovative targeted and immunotherapeutic strategies.

Recently, Wu et al. created a novel CD70-targeted tracer, [^{18}F]RCCB6, highlighting the utility of immuno-PET/CT for assessing tumor burden and monitoring treatment responses in patients with advanced ccRCC (*23*,*24*). In addition to CD70, CAIX also has demonstrated promising efficacy in theranostics for ccRCC. For example, Turkbey et al. conducted a phase II pilot study of [^{18}F]F-VM4–037 and found that the tracer posed challenges in evaluating primary ccRCC lesions (*25*). Kulterer et al. studied the performance of [^{99m}Tc]Tc-PHC-102, administering a high dose of the tracer to each patient (600–800 MBq) (*26*).

In this study, we developed the radiotracer [^{68}Ga]Ga–NYM046, characterized by satisfactory purity and stability. Compared with NY104, which also features acetazolamide as its base structure, NYM046 shows similar CAIX-targeting affinity (4.98 nM vs. 5.75 nM) and reduced uptake in normal tissues, including kidney, lung, and bone, as observed in animal models (*27*). In patients, [^{68}Ga]Ga-NYM046 PET/CT detected all primary tumors (9/9), whereas [^{68}Ga]Ga-NY104 PET/CT showed an accuracy of only 58% (11/19) in cases of a primary renal mass (*28*). The main structural distinctions between NY104 and NYM046 are the incorporation of a DOTA macrocycle and a naphthyl group. DOTA and its derivatives are known to form highly stable complexes with ^{68}Ga (*29*,*30*). Furthermore, previous studies on PSMA-617 have shown that incorporating a naphthylic linker significantly enhances tumor targeting and biologic activity and could help to optimize pharmacokinetics and improve imaging contrast (*31*,*32*). In the blocking assay, unlabeled NYM046 effectively inhibited binding of [^{68}Ga]Ga-NYM046 to CAIX, further confirming its targeting specificity.

In the clinical study, [^{68}Ga]Ga-NYM046 was highly concentrated in the kidneys because of eventual excretion through the urinary system, and it showed high accumulation in the stomach because of the physiologically high expression of CAIX in the human gastric mucosa (*33*). In a lesion-based analysis, [^{68}Ga]Ga-NYM046 PET/CT detected more primary and metastatic lesions of ccRCC than did conventional CT or ^{18}F-FDG PET/CT. [^{68}Ga]Ga-NYM046 uptake was typically higher than ^{18}F-FDG uptake in primary tumors but was lower in involved lymph nodes and comparable in distant metastases. One reason is that immune

cells are an important component of the tumor microenvironment and are present at all stages of tumorigenesis (*34*). Particularly in ^{18}F-FDG PET/CT, inflammation and the associated reactive activation of tissues can lead to nonspecific uptake in immune cells (*35*).

Furthermore, this study revealed a positive correlation between the expression of CAIX and the SUV_{max} of [^{68}Ga]Ga-NYM046. However, the regulation of CAIX expression is predominantly governed by HIF-α–mediated mechanisms. Considering that hypoxia often occurs in solid tumors (*36*,*37*), it is important to be aware of the risk for secondary malignancies, with prostate, breast, colon, bladder cancers, and non-Hodgkin lymphoma being the 5 most common secondary malignancies in certain individuals with ccRCC (*38*). From another perspective, this insight suggests that tracers targeting CAIX may offer a broader scope of clinical utility, extending beyond the traditional association with ccRCC (Supplemental Fig. 7). Further research will be necessary to explore this potential.

The field of integrated diagnostic and therapeutic tracers is gaining increasing prominence. Radiopharmaceutical therapy with [^{177}Lu]Lu-PSMA-617, used in patients with PSMA-positive metastatic castration-resistant prostate cancer, has shown efficacy in prolonging progression-free and overall survival (*39*). Consequently, NYM046, which contains a DOTA structure for stable binding with ^{177}Lu, holds certain potential for radiopharmaceutical therapy. However, the aggregation of NYM046 in the gastric mucosa may raise concerns about potential normal-tissue injury and warrants further investigation in future studies.

This study had some limitations. First, the study's small sample of patients may introduce statistical bias. Second, because of the potential side effects of invasive examinations, the metastatic lesions in the patients were not pathologically confirmed, potentially leading to diagnostic errors. We anticipate addressing these issues in future research.

CONCLUSION

We successfully developed a CAIX-targeting small-molecule tracer, [^{68}Ga]Ga-NYM046, that might offer a practical approach for diagnosing and monitoring treatment efficacy in patients with ccRCC.

KEY POINTS

QUESTION: Does [^{68}Ga]Ga-NYM046, a novel CAIX-targeted PET tracer, perform better than ^{18}F-FDG in the diagnosis of ccRCC?

PERTINENT FINDINGS: In a prospective study of 12 patients with ccRCC, [^{68}Ga]Ga-NYM046 PET/CT was superior to ^{18}F-FDG PET/CT in the diagnosis of primary tumors and comparable in the detection of metastatic lesions.

IMPLICATIONS FOR PATIENT CARE: [^{68}Ga]Ga-NYM046 provides a promising method for diagnosing and monitoring treatment efficacy in patients with ccRCC.

DISCLOSURE

This work was supported by the Subject Construction Fund from the Wuxi Medicine School of Jiangnan University, the Subject Development Fund (FZXK2021011) from the Wuxi Health Select Committee, and the Clinical Research and Translational Medicine Research Fund (LCYJ202331) from the Affiliated Hospital of Jiangnan University. No other potential conflict of interest relevant to this article was reported.

ACKNOWLEDGMENTS

We thank the clinical and research staff at the Department of Nuclear Medicine, Affiliated Hospital of Jiangnan University, for technical assistance and helpful discussions. We also thank Norroy Bioscience for professional technical assistance.

REFERENCES

1. Sung H, Ferlay J, Siegel RL, et al. Global cancer statistics 2020: GLOBOCAN estimates of incidence and mortality worldwide for 36 cancers in 185 countries. *CA Cancer J Clin.* 2021;71:209–249.
2. Rathmell WK, Rumble RB, Van Veldhuizen PJ, et al. Management of metastatic clear cell renal cell carcinoma: ASCO guideline. *J Clin Oncol.* 2022;40:2957–2995.
3. Edge SB, Compton CC. The American Joint Committee on Cancer: the 7th edition of the AJCC cancer staging manual and the future of TNM. *Ann Surg Oncol.* 2010;17:1471–1474.
4. Patel U, Sokhi H. Imaging in the follow-up of renal cell carcinoma. *AJR.* 2012;198:1266–1276.
5. Sivaramakrishna B, Gupta NP, Wadhwa P, et al. Pattern of metastases in renal cell carcinoma: a single institution study. *Indian J Cancer.* 2005;42:173–177.
6. Scatarige JC, Sheth S, Corl FM, Fishman EK. Patterns of recurrence in renal cell carcinoma: manifestations on helical CT. *AJR.* 2001;177:653–658.
7. Wang HY, Ding HJ, Chen JH, et al. Meta-analysis of the diagnostic performance of [^{18}F]FDG-PET and PET/CT in renal cell carcinoma. *Cancer Imaging.* 2012;12:464–474.
8. Majhail NS, Urbain JL, Albani JM, et al. F-18 fluorodeoxyglucose positron emission tomography in the evaluation of distant metastases from renal cell carcinoma. *J Clin Oncol.* 2003;21:3995–4000.
9. Long NM, Smith CS. Causes and imaging features of false positives and false negatives on F-PET/CT in oncologic imaging. *Insights Imaging.* 2011;2:679–698.
10. Fuccio C, Ceci F, Castellucci P, et al. Restaging clear cell renal carcinoma with ^{18}F-FDG PET/CT. *Clin Nucl Med.* 2014;39:e320–e324.
11. Dorai T, Sawczuk IS, Pastorek J, Wiernik PH, Dutcher JP. The role of carbonic anhydrase IX overexpression in kidney cancer. *Eur J Cancer.* 2005;41:2935–2947.
12. Pastorekova S, Gillies RJ. The role of carbonic anhydrase IX in cancer development: links to hypoxia, acidosis, and beyond. *Cancer Metastasis Rev.* 2019;38:65–77.
13. Bismar TA, Bianco FJ, Zhang H, et al. Quantification of G250 mRNA expression in renal epithelial neoplasms by real-time reverse transcription-PCR of dissected tissue from paraffin sections. *Pathology.* 2003;35:513–517.
14. Liao S-Y, Lerman MI, Stanbridge EJ. Expression of transmembrane carbonic anhydrases, CAIX and CAXII, in human development. *BMC Dev Biol.* 2009;9:22.
15. Oosterwijk E, Bander NH, Divgi CR, et al. Antibody localization in human renal cell carcinoma: a phase I study of monoclonal antibody G250. *J Clin Oncol.* 1993;11:738–750.
16. Verhoeff SR, Oosting SF, Elias SG, et al. [^{89}Zr]Zr-DFO-girentuximab and [^{18}F]FDG PET/CT to predict watchful waiting duration in patients with metastatic clear-cell renal cell carcinoma. *Clin Cancer Res.* 2023;29:592–601.
17. Merkx RIJ, Lobeek D, Konijnenberg M, et al. Phase I study to assess safety, biodistribution and radiation dosimetry for ^{89}Zr-girentuximab in patients with renal cell carcinoma. *Eur J Nucl Med Mol Imaging.* 2021;48:3277–3285.
18. Muselaers CH, Boerman OC, Oosterwijk E, Langenhuijsen JF, Oyen WJ, Mulders PF. Indium-111-labeled girentuximab immunoSPECT as a diagnostic tool in clear cell renal cell carcinoma. *Eur Urol.* 2013;63:1101–1106.
19. Verhoeff SR, van Es SC, Boon E, et al. Lesion detection by [^{89}Zr]Zr-DFO-girentuximab and [^{18}F]FDG-PET/CT in patients with newly diagnosed metastatic renal cell carcinoma. *Eur J Nucl Med Mol Imaging.* 2019;46:1931–1939.
20. Zhong L, Li Y, Xiong L, et al. Small molecules in targeted cancer therapy: advances, challenges, and future perspectives. *Signal Transduct Target Ther.* 2021;6:201.
21. Moch H, Cubilla AL, Humphrey PA, Reuter VE, Ulbright TM. The 2016 WHO classification of tumours of the urinary system and male genital organs: part A—renal, penile, and testicular tumours. *Eur Urol.* 2016;70:93–105.
22. Barata PC, Rini BI. Treatment of renal cell carcinoma: current status and future directions. *CA Cancer J Clin.* 2017;67:507–524.

23. Wu Q, Wu Y, Zhang Y, et al. ImmunoPET/CT imaging of clear cell renal cell carcinoma with [^{18}F]RCCB6: a first-in-human study. *Eur J Nucl Med Mol Imaging.* 2024;51:2444–2457.
24. Wu Q, Wu Y, Zhang Y, et al. [^{18}F]RCCB6 immuno-positron emission tomography/computed tomography for postoperative surveillance in clear cell renal cell carcinoma: a pilot clinical study. *Eur Urol.* 2024;86:372–374.
25. Turkbey B, Lindenberg ML, Adler S, et al. PET/CT imaging of renal cell carcinoma with ^{18}F-VM4-037: a phase II pilot study. *Abdom Radiol (NY).* 2016;41:109–118.
26. Kulterer OC, Pfaff S, Wadsak W, et al. A microdosing study with ^{99m}Tc-PHC-102 for the SPECT/CT imaging of primary and metastatic lesions in renal cell carcinoma patients. *J Nucl Med.* 2021;62:360–365.
27. Zhu W, Li X, Zheng G, et al. Preclinical and pilot clinical evaluation of a small-molecule carbonic anhydrase IX targeting PET tracer in clear cell renal cell carcinoma. *Eur J Nucl Med Mol Imaging.* 2023;50:3116–3125.
28. Zhu W, Zheng G, Yan X, et al. Diagnostic efficacy of [^{68}Ga]Ga-NY104 PET/CT to identify clear cell renal cell carcinoma. *Eur J Nucl Med Mol Imaging.* June 25, 2024 [Epub ahead of print].
29. Guleria M, Das T, Amirdhanayagam J, Sarma HD, Dash A. Comparative evaluation of using NOTA and DOTA derivatives as bifunctional chelating agents in the preparation of ^{68}Ga-labeled porphyrin: impact on pharmacokinetics and tumor uptake in a mouse model. *Cancer Biother Radiopharm.* 2018;33:8–16.
30. Tsionou MI, Knapp CE, Foley CA, et al. Comparison of macrocyclic and acyclic chelators for gallium-68 radiolabelling. *RSC Advances.* 2017;7:49586–49599.
31. Benešová M, Schäfer M, Bauder-Wüst U, et al. Preclinical evaluation of a tailor-made DOTA-conjugated PSMA inhibitor with optimized linker moiety for imaging and endoradiotherapy of prostate cancer. *J Nucl Med.* 2015;56:914–920.
32. Lundmark F, Olanders G, Rinne SS, Abouzayed A, Orlova A, Rosenström U. Design, synthesis, and evaluation of linker-optimised PSMA-targeting radioligands. *Pharmaceutics.* 2022;14:1098.
33. Thiry A, Dogné JM, Masereel B, Supuran CT. Targeting tumor-associated carbonic anhydrase IX in cancer therapy. *Trends Pharmacol Sci.* 2006;27:566–573.
34. Greten FR, Grivennikov SI. Inflammation and cancer: triggers, mechanisms, and consequences. *Immunity.* 2019;51:27–41.
35. Demmert TT, Pomykala KL, Lanzafame H, et al. Oncologic staging with ^{68}Ga-FAPI PET/CT demonstrates a lower rate of nonspecific lymph node findings than ^{18}F-FDG PET/CT. *J Nucl Med.* 2023;64:1906–1909.
36. Robertson N, Potter C, Harris AL. Role of carbonic anhydrase IX in human tumor cell growth, survival, and invasion. *Cancer Res.* 2004;64:6160–6165.
37. Becker HM. Carbonic anhydrase IX and acid transport in cancer. *Br J Cancer.* 2020;122:157–167.
38. Rabbani F, Reuter VE, Katz J, Russo P. Second primary malignancies associated with renal cell carcinoma: influence of histologic type. *Urology.* 2000;56:399–403.
39. Sartor O, de Bono J, Chi KN, et al. Lutetium-177-PSMA-617 for metastatic castration-resistant prostate cancer. *N Engl J Med.* 2021;385:1091–1103.